THE JOURNAL OF BIOLOGICAL CHEMISTRY VOL. 282, NO. 24, pp. 17720–17728, June 15, 2007

Interaction Sites between the *Slo1* Pore and the NH_2 Terminus of the β2 Subunit, Probed with a Three-residue Sensor*[S]

Received for publication, July 25, 2006, and in revised form, February 7, 2007 Published, JBC Papers in Press, April 12, 2007, DOI 10.1074/jbc.M607063200

Hui Li[‡1], Jing Yao[‡1], Xiaotian Tong[§], Zhaohua Guo[‡], Ying Wu[‡], Liang Sun[‡], Na Pan[‡], Houming Wu[§], Tao Xu[‡¶2], and Jiuping Ding[‡3]

From the [‡]Institute of Biochemistry and Biophysics, College of Life Science and Technology, Huazhong University of Science and Technology, Wuhan, Hubei 430074, China, the [¶]National Laboratory of Biomacromolecules, Institute of Biophysics, Chinese Academy of Science, Beijing 100101, China, and the [§]State Key Laboratory of Bio-organic and Natural Products Chemistry, Shanghai Institute of Organic Chemistry, Chinese Academy of Sciences, Shanghai 200032, China

Calcium- and voltage-gated (BK) K^+ channels encoded by *Slo1* play an essential role in nervous systems. Although it shares many common features with voltage-dependent K_V channels, the BK channel exhibits differences in gating and inactivation. Using a mutant in which FWI replaces three residues (FIW) in the NH_2 terminus of wild-type β2-subunits, in conjunction with alanine-scanning mutagenesis of the *Slo1* S6 segment, we identify that the NH_2 terminus of β2-subunits interacts with the residues near the cytosolic superficial mouth of BK channels during inactivation. The cytosolic blockers did not share the sites with NH_2 terminus of β2-subunits. A novel blocking-inactivating scheme was proposed to account for the observed non-competition inactivation. Our results also suggest that the residue Ile-323 plays a dual role in interacting with the NH_2 terminus of β2-subunits and modulating the gating of BK channels.

Ca^{2+} and voltage-gated K^+ channels (BK channels)[4] are encoded by mammalian *Slo1* genes related to the *Drosophila Slowpoke* (*Slo*) gene (1, 2). These channels are abundantly distributed in the nervous system to regulate excitability in response to intracellular Ca^{2+} and membrane potential. Rapid inactivation of BK channels results from *mSlo1* pore-forming α-subunits being coexpressed with auxiliary β2-subunits (3–6).

BK channels probably share similar pore structural determinants and many kinetic characteristics with voltage-dependent K^+ channels (K_V channels). For K_V channels, N-type inactivation arises from the cytosolic NH_2 terminus of the pore-forming α-subunits (7, 8) or the auxiliary β-subunits (9) inserting into the ion permeation pathway thereby blocking conduction ion permeation. Previous studies show that the NH_2 terminus of either the α- or β-subunit requires an inactivation domain (ID) composed of a hydrophobic head group to inactivate channels, followed by several positively charged amino acids (10, 11). Xia *et al.* (12) reported that the uncharged hydrophobic head group (FIW) of the hβ2 NH_2 terminus results in the inactivation of BK channels and proves that it is the only structural determinant required for inactivation.

Evidence supporting the idea that the ID must insert into the pore is derived from the blocking experiments of K_V channels by cytosolic blockers, which compete with the ID for channel occupancy (13, 14), thus resulting in the slowing of inactivation kinetics. Another report from McKinnon's laboratory (15) demonstrated that the first four residues of the NH_2 terminus of an inactivating $K_V\beta$ auxiliary subunit indeed interact with pore-lining residues of the K_V1.4 α-subunit. By contrast with K_V channels, cytosolic blockers of BK channels do not slow the inactivation kinetics, indicating that there is no competition between these blockers and the ID of hβ2-subunits (3, 16, 17). For BK channels, there are two questions to be left, that is, how the ID interacts with the channel pore and why the cytosolic blocker of BK channels does not compete with the ID.

With a mutant FWI, which is obtained from substituting the initial three amino acids (FIW) of the hβ2-subunit NH_2 terminus with FWI, and a systematic alanine-scanning mutagenesis of the *mSlo1* S6 segment, we demonstrate that the residue Ile-323 of *mSlo1* α-subunits plays a dual role in interacting with the ID of hβ2-subunits and modulating the gating of BK channels. We examined the binding sites of both the cytosolic blockers and the ID of hβ2-subunits and developed a new model for explaining the non-competition mechanism of inactivating BK channels. The present findings may underlie the gating and inactivating mechanisms of BK channels.

EXPERIMENTAL PROCEDURES

Site-directed Mutagenesis—All mutations of *mSlo1* and hβ2 were generated through PCR reactions, and all constructs were verified by sequencing. The FWI mutation of the wild-type hβ2

* This work was supported by the National Science Foundation of China (Grants 30470449, 30630020, 30670502, 30470646, 30500117, and 20132030), the Major State Basic Research Program of P. R. China (Grant 2004CB720000), and the Chinese Academy of Sciences (Grant KGCX2-SW-213-05). The costs of publication of this article were defrayed in part by the payment of page charges. This article must therefore be hereby marked "*advertisement*" in accordance with 18 U.S.C. Section 1734 solely to indicate this fact.

[S] The on-line version of this article (available at http://www.jbc.org) contains supplemental Figs. S1 and S2 and Tables S1 and S2.

[1] Both authors contributed equally to this work.
[2] To whom correspondence may be addressed: Tel.: 86-10-6488-8469; Fax: 86-10-6486-7566; E-mail: xutao@ibp.ac.cn.
[3] To whom correspondence may be addressed: Tel.: 86-27-8779-2153; Fax: 86-27-8779-2024; E-mail: jpding@mail.hust.edu.cn.

[4] The abbreviations used are: BK channel, Ca^{2+} and voltage-gated K^+ channel; K_V channel, voltage-dependent K^+ channel; ID, inactivation domain; TEA, tetraethylammonium; TM, transmembrane; HEDTA, *N*-hydroxyethylenediaminetriacetic acid.

was generated by the traditional PCR reaction with the primers 5′-GCGCAAGCTTACCACCATGTTTTGGATAACCAGTGGCCGGACCTCTTCATC-3′ and 5′-GGCCCTCGAGTTATCTATTGATCCGTTGGATCCTCTCAC-3′.

The product was digested with HindIII and XhoI and then ligated into HindIII_XhoI vector pBF. Other point mutations of *mSlo1* and hβ2 were generated by QuikChange protocol (Stratagene). For example, PCR reactions of *mSlo1* were performed with *mSlo1* as a template and a pair of complementary mutagenesis primers. The PCR reaction mixture was then cut with the enzyme DpnI to digest the template *mSlo1*. After DpnI digestion, the PCR mixture was used to transform competent bacterial cells to amplify the mutant plasmid of *mSlo1*.

Expression in Xenopus Oocytes—After DNA was linearized with MluI, SP6 RNA polymerase (Roche Applied Science) was used to synthesize cRNA for oocyte injection. The stage V–VI *Xenopus* oocytes were injected with 5–10 ng of cRNAs and then incubated in ND-96 solution at 18 °C for 2–7 days. To keep β2 (or β2 mutants)-subunits at a saturating concentration, we co-injected *mSlo1* α (or α mutants) and β2 (or β2 mutants) mRNAs into oocytes in a ratio of at least 1:2 by weight.

Electrophysiology—Macroscopic currents were recorded in inside-out patches at room temperature (22–25 °C). Pipettes were filled with a solution containing the following (in millimolar): 160 $MeSO_3K$, 10 H^+-HEPES, and 2 $MgCl_2$, adjusted to pH 7.0 with $MeSO_3H$. Intracellular solutions with different free [Ca^{2+}] were made by mixing 160 mM $MeSO_3K$ and 10 mM H^+-HEPES with $Ca(MeS)_2$ and 5 mM HEDTA (for 10 μM) or 5 mM EGTA (for 0 μM). Free [Ca^{2+}] was defined by the EGTAETC program (E. McCleskey, Vollum Institute, Portland, OR), with the pH adjusted to 7.0. Patch pipettes pulled from borosilicate glass capillaries had resistances of 2–6 MΩ when filled with internal solution. Experiments were performed and recorded using an EPC-9 patch clamp amplifier and PULSE software (HEKA Elektronic, Lambrecht/Pfalz, Germany). Currents were typically digitized at 20 kHz. All macropatch records were filtered at 2.9-kHz during digitization. For displays, currents were filtered digitally at 2 kHz (Bessel 8-pole). All single-channel currents were recorded at 10 kHz. During recording, solutions with or without the drugs QX-314 (2 mM) or tetraethylammonium (TEA, 50 mM) were puffed locally onto the inside-out patches via a puffer pipette containing seven solution tubes. The tip (~300 μm diameter) of the puffer pipette was located about 120 μm from the patches. As determined by the conductance tests, the solution around a patch under study was fully controlled by the application of a solution with a flow rate of 100 μl/min or greater. All pharmacological experiments met this criterion. Chemicals were obtained from Sigma-Aldrich.

Data Analysis—Data were analyzed with IGOR (Wavemetrics, Lake Oswego, OR), Clampfit (Axon Instruments, Foster City, CA), and SigmaPlot (SPSS Science, Chicago, IL) software. Unless stated otherwise, the data are presented as mean ± S.E., significance was tested by Student's *t* test, and differences between the mean values were considered significant at a probability of ≤0.05. *G–V* curves for activation were generated from steady-state currents, converted to conductance and then fitted by the single Boltzmann function with the form,

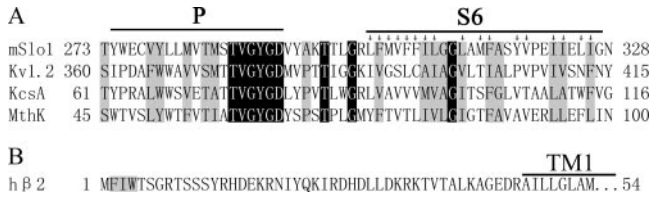

FIGURE 1. **Multisequence alignment within the pore region of *mSlo1* and three other K_V channels and a sequence of the NH_2 terminus of hβ2 used in this study.** *A*, the predicted domains of the P loop and the pore region of the S6 segment of the *mSlo1* gene are marked with *lines above*. Residues in which the nature of the side chain is preserved (>50% similarity) are marked in *gray* and homologous residues in *black*. The *arrows* in the *mSlo1* S6 domain refer to the amino acids we mutated into alanine. The sequences are: *mSlo1*, *Mus musculus*, accession number (acc) PIR A48206; K_V1.2, *Rattus norvegicus*, acc PIR NM_012970; KcsA, *Streptomyces lividans*, acc PIR S60172; MthK, *Methanothermobacter thermautotrophicus*, acc PIR AAB85995. *B*, sequence of NH_2 terminus of the *mSlo1* auxiliary hβ2-subunits. *TM1* designates the proposed beginning of the first TM segment. The first three hydrophobic residues FIW, which induce inactivation of BK channels (12), are shown in *gray*. The sequence is: hβ2, human KCNMB2, acc PIR NM_005832.

$$G/G_{max} = (1 + \exp((v - v_{50})/\kappa))^{-1} \quad \text{(Eq. 1)}$$

where V_{50} is the voltage at which the conductance (G) is half the maximum conductance (G_{max}), and κ is a factor affecting the steepness of the activations. Recovery curves were fitted with the bi-exponential function (Equation 2),

$$\text{Fractional recovery} = a_{fast} \times (1 - \exp(t/\tau_{fast})) + a_{slow} \times (1 - \exp(-t/\tau_{slow})) \quad \text{(Eq. 2)}$$

where a_{fast}, τ_{fast}, a_{slow}, and τ_{slow} are the percentages and time constants of fast and slow recovery components, respectively. The first term on the right of Equation 2 was used for the mono-exponential recovery.

RESULTS

The Mutation FWI Is a More Sensitive Probe for Screening the Interaction Sites—The pore-forming segment (S6) of the α-subunits of BK channels shares homology with the K^+ channels, several of whose crystal structures have been well resolved (18–20). After aligning the sequences of *mSlo1* with the potassium channels KcsA, K_V1.2, and MthK (Fig. 1*A*), we inferred by structural homology that the pore-lining residues in BK channels were Ile-323, Val-319, Phe-315, and Leu-312 (18). The hβ2-subunit of the BK α-subunit has two proposed transmembrane (TM) segments with an intracellular NH_2 terminus of 46 amino acids (3). The sequence of the hβ2 NH_2 terminus followed by the predicted first transmembrane (TM1) segment is given in Fig. 1*B*.

To determine interaction between the ID and pore, the wild-type hβ2 (FIW) usually serves for detecting the interacting residues in the pore by means of alanine mutagenesis of *mSlo1* α-subunits. The time constant of recovery from inactivation is a good character for this purpose. On the basis of our preliminary results, however, it is difficult to use the FIW to determine the interacting sites due to its doubtful time constants in recovery from inactivation (data not shown). Therefore, it is necessary to find a more sensitive probe for the goal mentioned previously.

After examining wild-type hβ2 (FIW) and three rearranged constructs FWI, IWF, and WIF, we find that they largely share

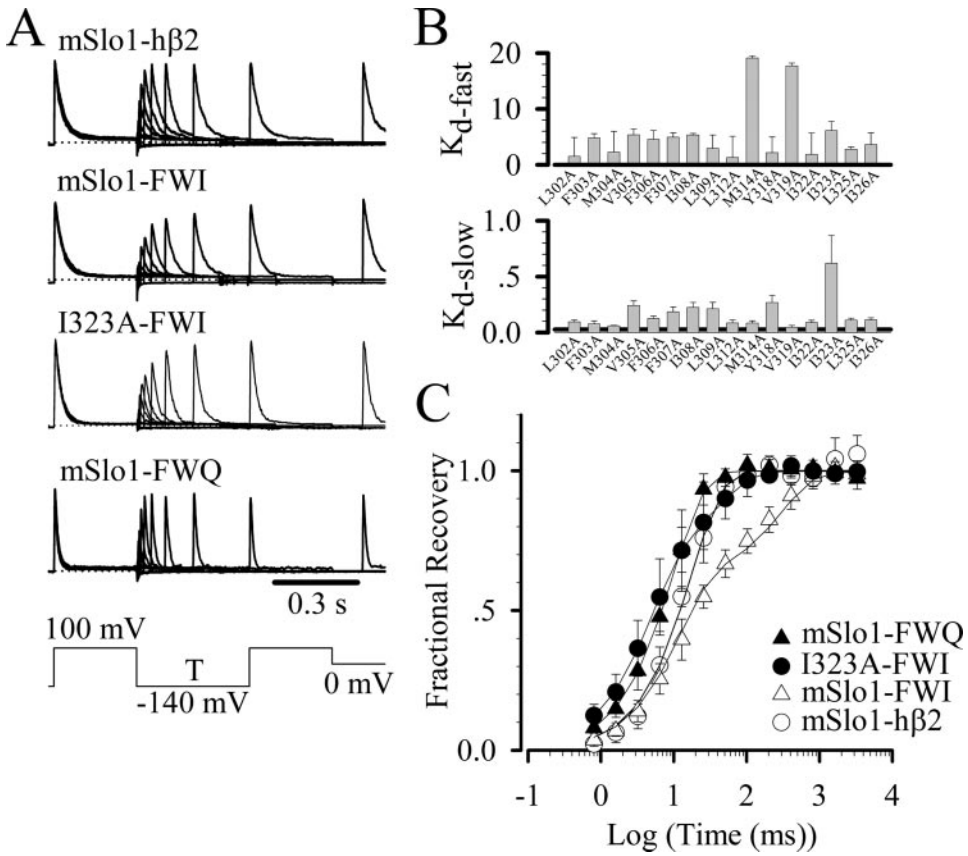

FIGURE 2. **Mutational analysis of the ID of hβ2-subunits and hydrophobic residues in the S6 pore region of *mSlo1* channels.** *A*, currents resulting from *mSlo1*-hβ2, *mSlo1*-FWI, I323A-FWI, and *mSlo1*-FWQ as indicated were activated by a paired pulse protocol with 10 μM Ca^{2+}. The voltage protocol is shown at the *bottom*. *T* is the variable time interval between the two pulses. The scale for currents is in arbitrary units. The *dotted line* is zero-current line. *B*, for all the *mSlo1* mutants coexpressed with FWI, the ratio $\tau_i/\tau_{r\text{-fast}}$ is referred as $K_{d\text{-fast}}$ (fast dissociation constant) and the ratio of $\tau_i/\tau_{r\text{-slow}}$ as $K_{d\text{-slow}}$ (slow dissociation constant). τ_i is the inactivation time constant measured at 100 mV with 10 μM Ca^{2+}, $\tau_{r\text{-fast}}$ is the fast component of the recovery time constant at −140 mV with 10 μM Ca^{2+} and $\tau_{r\text{-slow}}$ is the slow one. *C*, the fractional recovery as a function of recovery time is plotted for the set of traces in *A*. A single exponential function was fitted through the recovery points of hβ2-*mSlo1* (○, τ_r = 21.9 ± 4.8 ms; τ_i = 23.7 ± 2.9 ms; *n* = 10) and *mSlo1*-FWQ (▲, τ_r = 10.0 ± 1.7 ms; τ_i = 9.6 ± 1.2 ms; *n* = 8), and a bi-exponential function was fitted through the points of *mSlo1*-FWI (Δ, $\tau_{r\text{-fast}}$ = 6.5 ± 0.6 ms; $\tau_{r\text{-slow}}$ = 323.0 ± 46.0 ms; τ_i = 29.9 ± 2.7 ms; *n* = 5) and I323A-FWI (●, $\tau_{r\text{-fast}}$ = 4.4 ± 1.6 ms; $\tau_{r\text{-slow}}$ = 43.6 ± 22.3 ms; τ_i = 27.0 ± 8.0 ms; *n* = 8). The scale for currents is in arbitrary units.

most of kinetic characteristics in activation, inactivation, and recovery, except that the construct FWI exhibits a bi-exponential recovery different from the other mutations (12) (supplemental Fig. S1). For recovery from inactivation, the wild-type hβ2 and IWF and WIF exhibited similar time constants in a mono-exponential recovery (average τ_r = 18.5 ± 4.4 ms at −140 mV), whereas the mutation FWI exhibited bi-exponential recovery components with a fast component ($\tau_{r\text{-fast}}$ = 6.5 ± 0.6 ms at −140 mV) and a slow component ($\tau_{r\text{-slow}}$ = 323 ± 46 ms at −140 mV), ~50-fold slower (Fig. 2, *A* and *C*, and supplemental Table S1). We infer that the bi-exponential kinetics of FWI in recovery from inactivation mostly results from the residue Trp-3, because tryptophan is bulky and may have significant impact on the pore-lining residues in the S6 region during the recovery process. Despite the differences in the recovery kinetics, we believe that FWI interacts with a similar region of the channel as FIW, because their kinetic characteristics are very similar except for recovery.

Considering that the FWI as an infrequent mutation of the native hβ2 (FIW) exhibits a bi-exponential recovery, we infer that there should be a specific residue in the pore interacting with the FWI more strongly to induce the slow recovery. Furthermore, two components of FWI, especially the slow one, can be used to identify the interaction sites, and these are much better than one component of hβ2 (FIW). Comparing with the results from native hβ2 (FIW), we found in this study that the FWI was a better sensor for exploring interaction sites.

Residue Ile-323 in the Cavity of the mSlo1 Channel Interacts with the ID of the FWI—Because the ID produced inactivation through hydrophobic interaction, we systematically mutated each hydrophobic residue in S6 of BK channel to alanine. Each mutant of the *mSlo1* coexpressed with the mutation FWI was termed "mutant *mSlo1*-FWI," for example, I323A-FWI in this study. For each coexpression such as mutant *mSlo1*-FWI, all the recovery experiments were performed from inside-out patches by the paired-pulse recovery protocol shown at the *bottom* of Fig. 2*A* (Also see supplemental Fig. S2). Among the sixteen mutants of *mSlo1*, the coexpressed mutation I323A-FWI showed pronounced alterations in the slow dissociated constant $K_{d\text{-slow}}$, and the mutations V319A-FWI and M314A-FWI in the fast dissociated constant $K_{d\text{-fast}}$ (Fig. 2*B*). The slow recovery time constant of I323A-FWI $\tau_{r\text{-slow}}$ = 43.6 ms is the closest to the monoexponential recovery time constant of the wild-type *mSlo1*-hβ2 (τ_r = 21.9 ms). Considering the fact that the residue Ile-323 is a pore-lining residue, thus, we infer that Ile-323 possibly plays a significant role as one of the interaction sites in prolonging recovery from the inactivation. The fast recovery time constants of M314A-FWI and V319A-FWI ($\tau_{r\text{-fast}}^{M314A}$ = 1.9 ± 0.4 ms; $\tau_{r\text{-fast}}^{V319A}$ = 1.8 ± 0.5 ms) were significantly faster than those of any other mutations (supplemental Table S2). Both the amino acids Val-319 and Ile-323 probably contribute to the lining toward the inner wall of the pore, whereas the residue Met-314 may not (18). One explanation may be that the mutation M314A allosterically translocates the pore-lining residue Phe-315, which then may alter its contact with the ID of hβ2. Unfortunately, we failed to express mutant F315A (21), which may indicate an unusual structure between the Met-314 and Phe-315. An NMR structure of the hβ2 NH_2-terminal peptide (22) indicates that the first ten residues of hβ2 are flexible and extendable into a linear peptide structure. Making a rough estimate on the basis

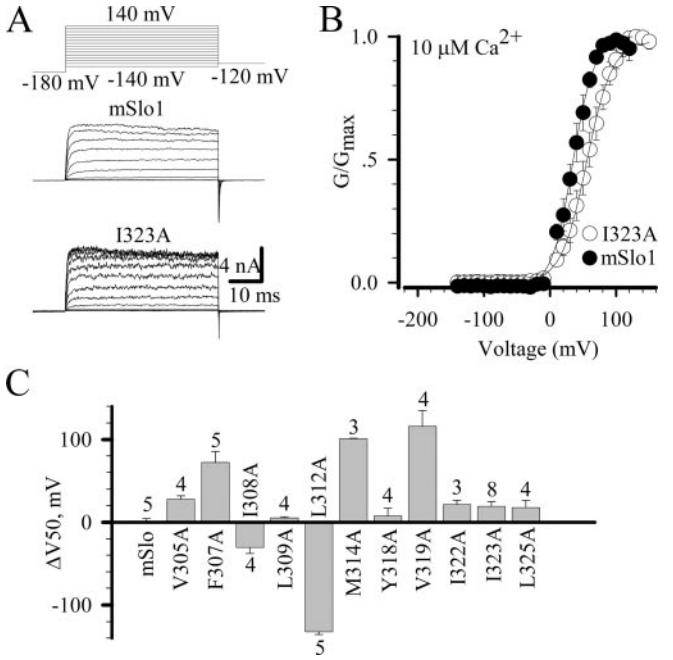

FIGURE 3. **Changes in the slow recovery component of the S6 pore mutations do not depend on *G–V* shifts.** *A*, the currents of the mutant I323A and the wild-type *mSlo1* activated by a voltage protocol as indicated at the top with intracellular 10 μM Ca^{2+}. *B*, *solid lines* are fits of the equation $G(V) = G_{max} \times (1 + \exp(V - V_{0.5})/k)^{-1}$. The fitted values for the $V_{0.5}$ are 36.0 ± 4.5 mV for *mSlo1* (●) (number of patches, $n = 5$) and 55.3 ± 5.7 mV for I323A (○) ($n = 8$). *C*, the relative change in $V_{0.5}$ between the *mSlo1* mutations and the wild-type *mSlo1* in the presence of 10 μM Ca^{2+}. Numbers of patches are given *above* or *below* the *bars*.

of an assumed linear inactivation peptide docked within the *mSlo1* ion conduction pathway, we hypothesize that Phe-2 in the ID of mutation FWI makes contact with Met-314, Trp-3 with Val-319, and Ile-4 with Ile-323 during the inactivation process.

Both Y318A-FWI and V305A-FWI show slow recovery time constants of over 80 ms, which are 4-fold that of *mSlo1*-hβ2 (22 ms) or 2-fold that of I323A-FWI (40 ms) (see supplemental Table S2). As the residue Tyr-318 is next to the pore-lining residue Val-319, we reckoned that it could interact with the ID also. For V305A, its influences were not so significant as the ones of the I323A or V319A in either slow or fast recovery components (Fig. 3). Secondly, the ID should interact with the residues clustering in a small group, not an isolated residue as Val-305 does. Finally, the structure model of *mSlo1* shows that the Val-305 in S6 might indirectly affect the slow recovery rate through forming a hydrophobic cluster with the neighboring residues in the S5 and S6. Thus, there is little possibility that Val-305 is one of the interaction sites with the ID.

To confirm the interaction between Ile-4 and Ile-323, we attempted to alter the hydrophobic residue Ile-4 in the FWI to a hydrophilic residue, *i.e.* a new mutant FWQ, to eliminate the slow recovery process. The fractional recovery from inactivation for *mSlo1*-FWQ and three other combinations of constructs are shown in Fig. 2*C*. Clearly, both the *mSlo1*-FWQ and *mSlo1*-hβ2 have only a single exponential recovery, but *mSlo1*-FWI exhibits two obvious exponential recovery components. Because the FWQ has the lesser hydrophobicity, the time constants of both recovery and inactivation of *mSlo1*-FWQ are faster than that of *mSlo1*-hβ2. The mono-exponential recovery curves of *mSlo1*-FWQ and *mSlo1*-hβ2 demonstrate a specific steric requirement for Ile-4 in the ID to directly interact with the pore-lining residue Ile-323.

We also compared the G-V curves of each pore mutation with the wild-type *mSlo1* and found that the V_{50} of I323A shifted only about +20 mV with 10 μM Ca^{2+} (Fig. 3*B*) relative to the *mSlo1*. Furthermore, we noticed that the relative V_{50} of the pore mutations compared with *mSlo1* shifted variously at 10 μM Ca^{2+} (Fig. 3*C*). Comparing Fig. 3*C* with Fig. 2*B*, we found that the slow recovery component was not tightly related to the changes of V_{50}, but mainly depended on the interaction between the pore and the ID. Taking L312A as an example, even though its V_{50} shifted ~−130 mV, the recovery of L312A still contained a slow recovery component.

No Mutations in the S6 Pore Significantly Affect the Binding Affinities of Cytosolic Blockers—Xia *et al.* (3) and Solaro *et al.* (17) reported that the cytosolic blockers of BK channels did not slow the inactivation process and further inferred that they did not share the binding sites with the ID based on the competition model of K_V channels. However, it is still unknown whether the blockers of BK channels have specific binding sites in pore and why they do not compete with the ID.

To determine whether blockers slow the inactivation process and where their binding sites are at the same time, we examined the inactivating currents of coexpression of the *mSlo1* mutants and FWI in most experiments. Cytosolic application of 2 mM QX-314 reduced the averaged peak currents to 20–50% but caused insignificant differences in inactivation time constants τ_i (Fig. 4, *A* and *B*). The inactivation time constants τ_i varied from 20 to 36 ms with an average time constant $\tau_i = 25.3 \pm 4.3$ ms. According to competition model, the 20–50% unblocking currents are predicted to produce a 2- to 4-fold slowing of τ_i (3, 13, 14). In Fig. 4 (*A* and *B*), however, 2 mM QX-314 resulted in no significant changes in τ_i for all the *mSlo1* mutants. Similar results were obtained by cytosolic application of 50 mM TEA (Fig. 4, *C* and *D*).

It seems unnecessary to use the FWI for determining the binding affinity of blockers. However, we will find something interesting after comparing how they differ. In Fig. 4*B*, 2 mM QX-314 showed less inhibition on the currents of the *mSlo1*-hβ2, M314A-FWI, and V319A-FWI than that of the *mSlo1*, M314A, and V319A, respectively, which suggests that the ID prevents QX-314 from entering the cavity. In Fig. 4*D*, however, 50 mM TEA did not show the statistic difference on inhibition probably due to a very high concentration used in this experiment. No matter whether we have used FWI or not, there is no significant difference in their binding affinities. It indicates that no mutations along the ion conduction pathway significantly affect the binding affinities of QX-314 or TEA.

A Kinetic Model for the Cytoplasmic Blocker QX-314 Blocking the Inactivating BK Channels—On the basis of our experiments, a schematic, which is presented with only two opposite subunits and one inactivation domain, illustrates a kinetic process that includes both the inactivation and the blocking and inactivation of BK channels (Fig. 5). For a competition model of K_V channels, the channel can only alter from the open state to the inactivated state or to the blocked state, but not to the

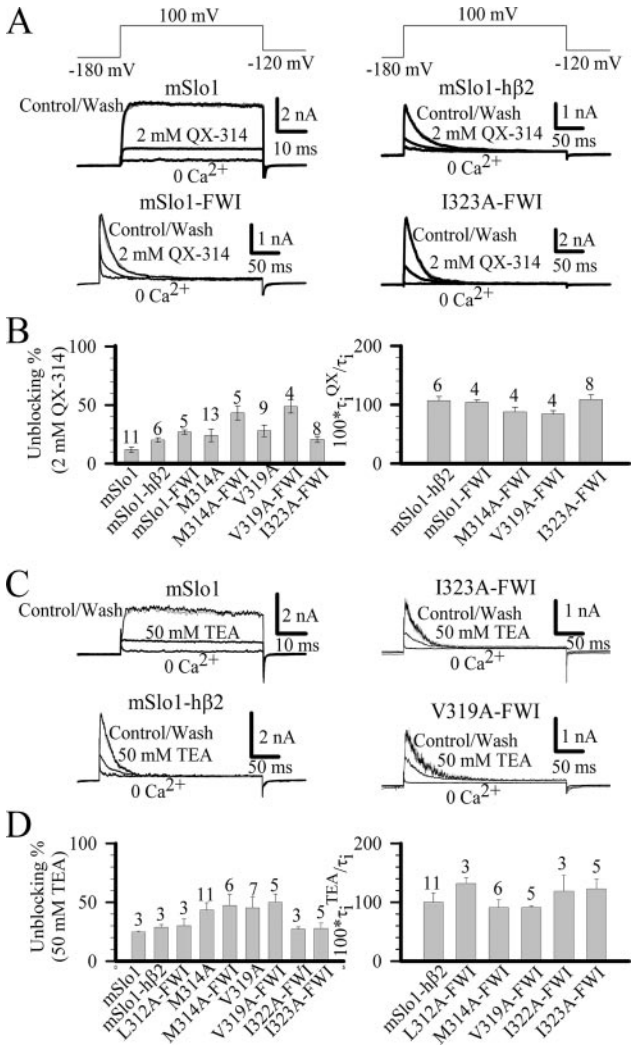

FIGURE 4. **The currents of mutations in the cavity of BK channels exhibit similar sensitivity to both QX-314 and TEA.** *A* and *C*, the representative traces of currents as indicated were elicited from inside-out patches in 10 μM Ca^{2+} by the voltage protocol shown at the *top*. Each *trace* is labeled with control/wash, 2 mM QX-314 (in *A*), 50 mM TEA (in *C*) and 0 μM Ca^{2+}, respectively. *B* and *D*, summary data showing the inhibitory effects of 2 mM QX-314 (in *B*) and 50 mM TEA (in *D*) on channel activity from *mSlo1*-hβ2, *mSlo1*-FWI and some of S6 mutations coexpressed with FWI. The *left panel* shows the fractional unblocking currents of *mSlo1* and other combinations as indicated. In *B* and *D*, the fractional unblocking currents of M314A and V319A were obtained at 300 μM Ca^{2+} and others at 10 μM Ca^{2+}. The *right panel* shows the ratio of $100*\tau_i^{QX\text{-}314}/\tau_i$ to allow a comparison between the inactivation time constants with and without QX-314 and TEA. The *number* on the *top* of the *bars* is the number of patches.

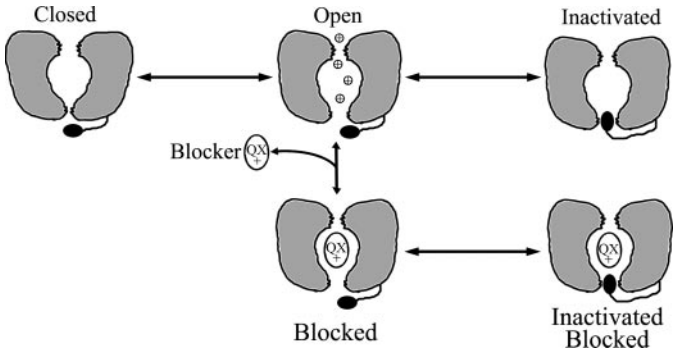

FIGURE 5. **Diagram of the one-step non-competition model accounting for the non-competitive blocking of BK channels by QX-314.**

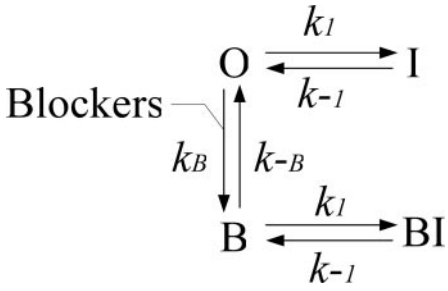

SCHEME 1

blocked and inactivated state, because the cytosolic blockers and the ID compete for binding to the same site (14).

In our non-competitive scheme for BK channels, the channel cannot only go from the open state to either the blocked state or the inactivated state, but also from the blocked state to the blocked and inactivated state. Therefore, the one-step non-competitive scheme for BK channels ("one-step" means one inactivation step) can be modeled as in Scheme 1, where states are represented by: O, open; I, inactivated; B, blocked; and BI, blocked-inactivated. Rate constants are: k_1, inactivation; k_{-1}, returning from inactivation; k_B, binding; and k_{-B}, dissociation.

The transition rates between the B and the BI states are same to that between the open (O) and the inactivated (I) states. There is no link between the BI and I states, because the charged blockers cannot penetrate through cell membrane. Therefore, blockers are trapped in the cavity of the pore when the inactivation site is occupied. Following Choi *et al.* (14), we also ignore the voltage-dependent activation steps, which are rapid and thus do not complicate measurements of inactivation at the positive voltages studied. For a complete inactivation, we make the assumption that k_{-1} is close to zero. The blockers association and dissociation is typically much more rapid than the inactivation process (*i.e.* k_B and $k_{-B} \gg k_1$). The channel goes to the inactivated state from the open state or to the blocked-inactivated state from the blocked state with the same inactivation time constant $\tau_i = 1/(k_1 + k_{-1})$ (for the case $k_1 \gg k_{-1}$, $\tau_i \approx 1/k_1$). The difference between the competitive and the non-competitive model is that the blocked channels are protected from rapid equilibrium with the pool of open channels and return to the blocking-inactivation state and "permanently" lost with the same rate as that between the open and inactivation state. Therefore, this scheme can predict that the inactivation time constant with and without blockade will be the same (the unblocked fraction of channels $f = k_{-B}/(k_B + k_{-B})$ and the inactivation time constant in the presence of blockers $\tau_i^{blocker} = 1/k_1$).

A similar consideration can be directly used to describe the two-step inactivation model. Two-step inactivation model (O ↔ O* ↔ I) is revised from the one-step inactivation model (O ↔ I) (13–16). O, O*, and I are the open, pre-inactivation, and inactivation states, respectively. However, the two-step inactivation model can be simplified into a one-step inactivation model when the transition rate between O and O* is much larger than between O* and I (15, 23).

Simulations in Fig. 6 illustrate two different cases, *i.e.* one-step non-competition and two-step non-competition. τ_c is defined as the control inactivation time constant (without

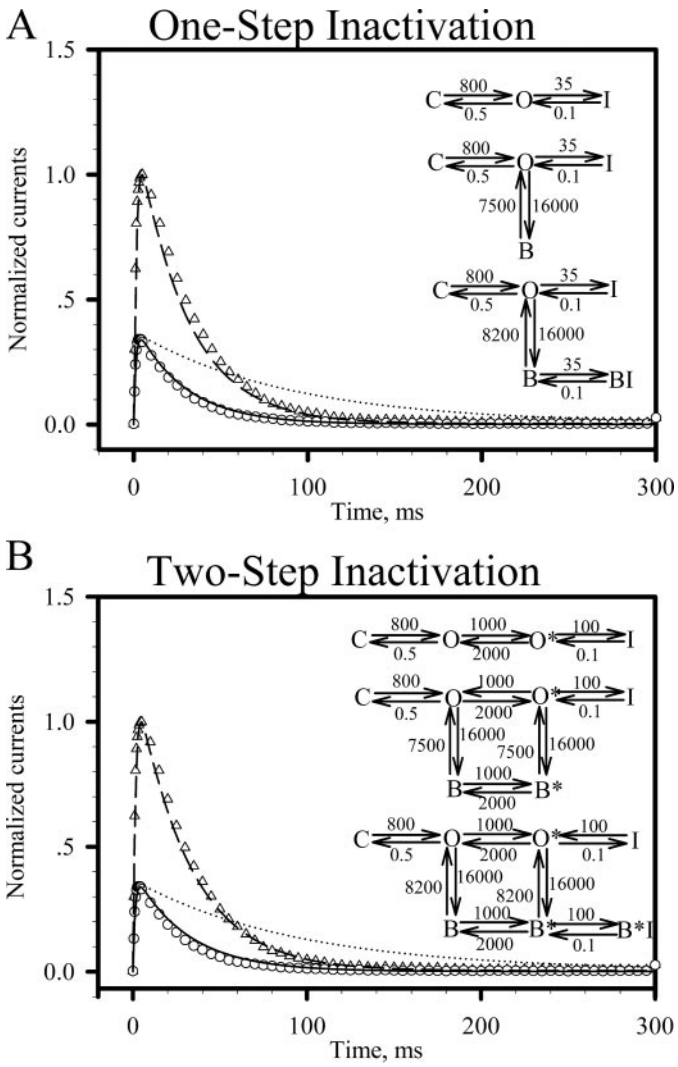

FIGURE 6. **Blocking-and-inactivation models for the blockade of QX-314 on the BK currents arising from the mutation F307A co-expressed with FWI.** *A*, for the one-step inactivation models, *triangles* and *circles* represent the currents evoked by a voltage step to 100 mV in the presence of 10 μM Ca^{2+} before and after applying 2 mM QX-314, respectively. The *long dash*, *dotted*, and *solid lines* represent the simulation traces calculated from the inactivation (*right top*), competition (*right middle*), and non-competition (*right bottom*) models, respectively. *B*, all the simulations were calculated from the two-step inactivation models shown on the *right side*. Other parameters are the same as those described in *A*.

blocker), τ_b is defined as the inactivation time constant at 2 mM QX-314, and f = max (unblocked)/max (control). In the simulation, we chose k_{OB} = 16,000, k_{BO} = 7,500 or 8,600 (24), $k_{OO}{}^*$ = 1,000, and $k_O{}^*{}_O$ = 2,000 (25). As long as the rates k_{OB} and k_{BO} are much larger than the other rates, the simulation always yields a non-competition result. From our experimental results, we have τ_c = 29.4 ms in *triangles*, τ_b = 25.3 ms in *circles*, and f = 0.3423. From the one-step inactivation simulation, we find τ_c = 28.7 ms (*long dashed line*) and τ_b = 88.8 ms (*dotted line*) for the competition model (f = 0.3453), τ_b = 28.5 ms (*solid line*) for the non-competition model (f = 0.3392). From the two-step inactivation simulation, we find τ_c = 30.8 ms (*long dashed line*), τ_b = 94.1 ms (*dotted line*) for the competition model (f = 0.3420), τ_b = 30.6 ms (*solid line*) for the non-competition model (f = 0.3392). The simulation results tallied extraordinarily well with our experimental data.

Residue Ile-323 Modulates the Gating of BK Channels—By analogy to the shaker-type K^+ channel K_V1.4-IR, residue Ile-323 in BK channels corresponds to Tyr-569 in K_V1.4-IR channels (15). Closer examination of I323A macroscopic and single-channel currents reveals additional critical differences from the wild-type BK channels. The I323A tail currents exhibit an outward rectified current, strikingly different from the wild-type channels (Fig. 7, *A* and *B*) (26). The results of the macroscopic currents are consistent with the outward rectification of unitary conductance measured from the maximum single-channel level shown in Fig. 7 (*C* and *D*). In contrast, the single-channel currents of the wild-type *mSlo1* show little rectification in Fig. 7 (*C* (*right*) and *D*). Resembling a *dSlo*-like flickery behavior (27, 28), the single channel of I323A shows very noisy opening in contrast to the *mSlo1* single-channel opening shown in Fig. 7*C*. We also observed that the open probability of the largest level reduced more rapidly at negative voltages. Consequently, the rectification property of the I323A mutant was possibly caused by the very short open time, the very low open probability, and the relatively low filtering frequency. More detailed work is clearly required to illuminate the nature of rectification. In addition, rectification will not affect the *G–V* curve due to very low open probability at negative voltages under conditions we currently used (Fig. 3*B*).

As the corresponding residue in the flickery *dSlo* (A2, C2, E2, G5, 10 splice variant) is Thr-337 rather than Ile (28, 29), we substituted Thr for Ile-323 in wide-type *mSlo1* and found that I323T induced the flickery single-channel currents similar to the flickery *dSlo*.[5] This mechanism may help us to understand the behavior of the flickery *dSlo* single channels.

Simulation of an Interaction between hβ2 (FIW and FWI) and mSlo1 Subunits of BK Channels—To further understand the molecular basis for interaction between the hβ2 subunit and BK-type channels, docking simulations were performed with the wild-type hβ2 (FIW) NH_2 terminus and its mutant FWI interacting with *mSlo1* α-subunits, using the bimolecular complex program 3D-DOCK (see also "Methods" in the supplemental materials). The most favorable docking conformations were guided by our experimental results described above (Fig. 8) based on the K_V1.2 channel data (PDB code 2A79) and the NMR data (PDB code 1JO6) of the hβ2 NH_2 terminus (22, 30). The computational models for complexes of FIW-*mSlo1* and FWI-*mSlo1* were further analyzed, using the LIGPLOT program (31, 32) (Fig. 9). As shown in Fig. 8, the FIW and FWI side chains of the hβ2 subunits are tightly packed together to form a hydrophobic core. Each component of the hydrophobic core makes close contact to a corresponding residue of the *mSlo1* S6 segment and fully blocks the mouth of the BK channels. The interactions in the *mSlo1*-hβ2 (*mSlo1*-FIW) structural model mainly involved hydrophobic contacts, which include Phe-2 with Val-319 (*B*), Ile-323 (*B*) and Val-319 (*D*), Ile-3 with P320 (*D*), and Trp-4 with Ile-323 (*C*). The interactions in the *mSlo1*-FWI structural model predict similar hydrophobic contacts: Phe-2 with Val-319 (*B*), Trp-3 with Ile-323 (*B*) and Ile-323 (*D*), and Ile-4 with Pro-320 (*B*) and Ile-323 (*C*). In addition, the

[5] H. Li, J. Yao, X. Tong, Z. Guo, Y. Wu, L. Sun, N. Pan, H. Wu, T. Xu, and J. Ding, unpublished data.

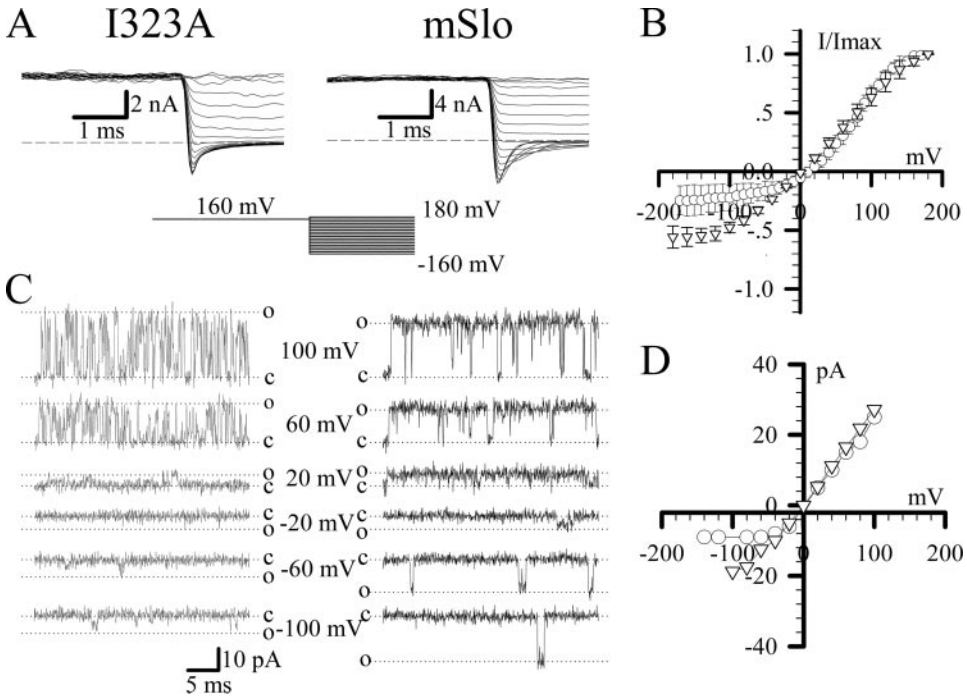

FIGURE 7. **Representative currents expressed with cRNA of I323A exhibit a flickery outward-rectified feather.** *A*, tail currents of I323A (*left*) and *mSlo1* (*right*) were activated by a voltage protocol, which is shown at the *bottom*, with intracellular 10 μM Ca^{2+}. The *dashed line* represents zero current. *B*, I–V curves are plotted based on the instantaneous values of tail currents (○, I323A; ▽, *mSlo1*; the number of patches is $n = 6$). The standard errors often lie *within the symbol*. *C*, representative single-channel currents of I323A (*left*) and *mSlo1* (*right*) show the maximum single-channel currents at voltages as indicated. *Dotted lines* labeled with a letter "*c*" represent the zero level, and those labeled with a letter "*o*" represent the maximum single-channel open level. All single-channel currents were recorded at 10 kHz. *D*, the I–V curves are plotted with the values of the maximum single-channel currents measured by eye (○, I323A ($n = 2$); *dotted line*, *mSlo1*).

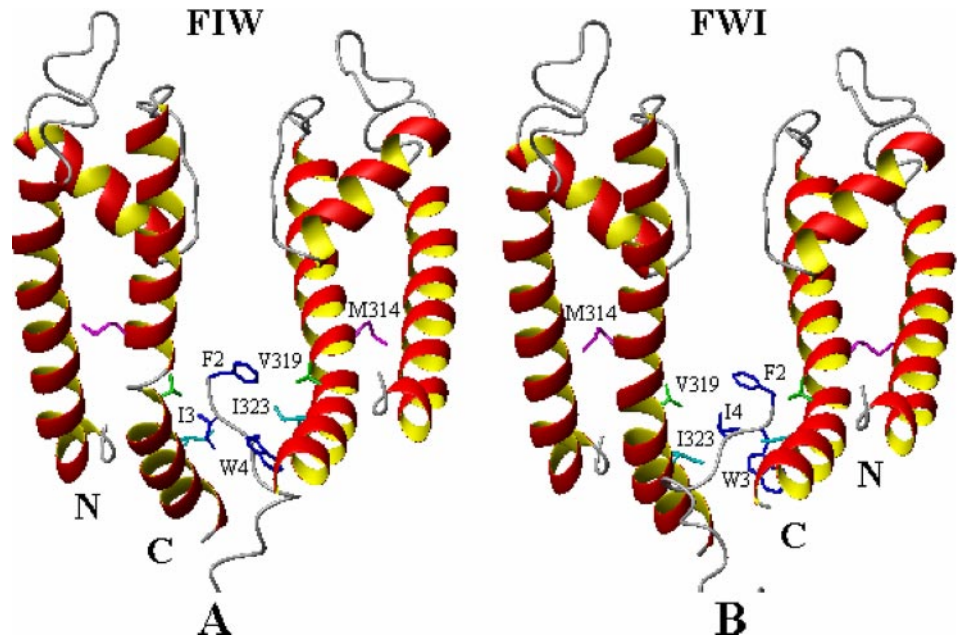

FIGURE 8. **The complex models of a channel composed of α subunit *mSlo1* and its auxiliary NH_2 terminus (hβ2) generated by 3D_DOCK program.** For clarity, two of the four subunits, B and D, for *mSlo1* and the NH_2-terminal segment of hβ2 are presented. *N* and *C* indicate NH_2 terminus and C terminus of one subunit of *mSlo1*, respectively. *A*, the structure of *mSlo1* with hβ2 (FIW). The interactions are mediated by hydrophobic contacts involving Phe-2 and Val-319 (*B*), Phe-2 and Ile-323 (*B*), Phe-2 and Val-319 (*D*), Ile-3 and Pro-320 (*D*), and Trp-4 and Ile-323 (*C*). *B*, The model of *mSlo1* with hβ2 (FWI). The closest contacts between the proteins mainly include Phe-2 and Val-319 (*B*), Trp-3 and Ile-323 (*B*), Trp-3 and Ile-323 (*D*), Ile-4 and Pro-320 (*B*), Ile-4 and Ile-323 (*C*), and Thr-5 and Ile-323 (*C*). The results suggest the interactions between *mSlo1* channel and hβ2 are mainly composed of hydrophobic contacts.

amino acid Thr-5 of the hβ2 in the *mSlo1*-FWI complex also predicts hydrophobic contacts with Ile-323 (*C*).

DISCUSSION

In this study, we show that the ID of the hβ2-subunit does not occupy the same site with channel blockers, which directly leads to a non-competitive inactivation. However, two critical questions need to be answered: why the channels in this work did not show any reopening during the deactivation process and by what pathway the ID can access the conducting entrance of the pore.

In K_V channels, once the ID occupies its blocking position, it impedes closure of the channels to lead channels to reopen during the deactivation process (8, 13). In BK channels, during the process of deactivation, the fully inactivated channels with a hydrophobic inactivation domain such as hβ2 do not show reopening but do show reopening with some lesser hydrophobic inactivation domains such as hβ3b. It seems to depend on whether the recovery time constant is comparable to the closing time constant. Because the recovery process of hβ2 from complete inactivation (*e.g.* 20 ms) is usually much slower than its closing process (*e.g.* 0.1 ms), thus it can fully conceal the reopen process of BK channels. By contrast, we can anticipate that the reopening appears from the incomplete inactivated BK channels by hβ3b with a recovery time constant of $\tau_r = 0.38$ ms.[5] Moreover, recent work from a few laboratories has shown that the ID reaches the ion-conducting pore through lateral "side portals" in the cytoplasmic portion of the channel (20, 33, 34). In our modeling, we cannot exclude any pathway accessing to or withdrawing from the ion-conducting pore.

Here we also want to emphasize that the models for both the competitive and non-competitive case may give a bi-exponential inactivation if the blocking rates are relatively smaller, that is, one of the inactivation time constants is faster

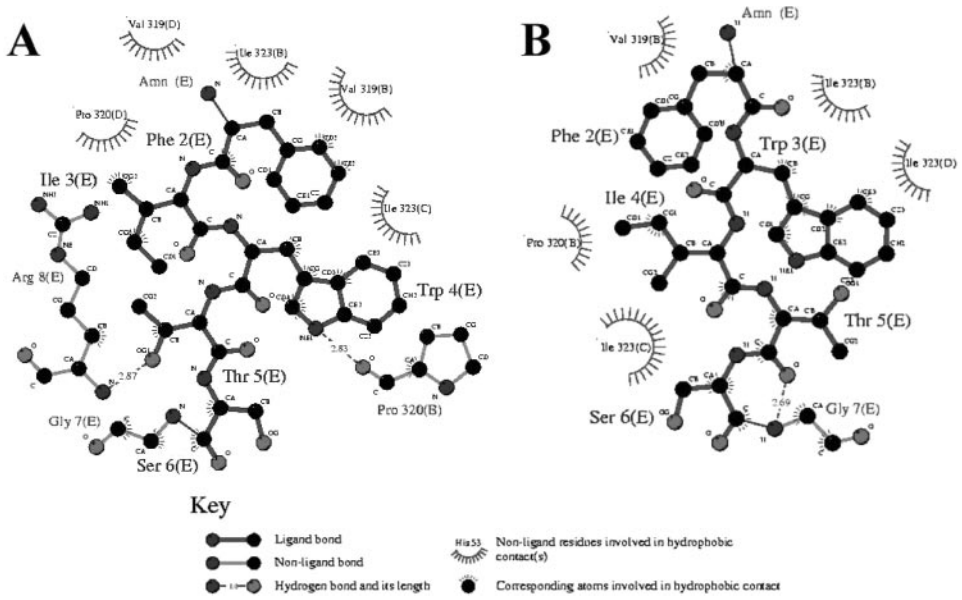

FIGURE 9. **A depiction (generated by LIGPLOT) of the main interactions involved in hβ2 (FIW)-*mSlo1* (*A*) and hβ2 (FWI)-*mSlo1* (*B*).**

and the another slower than the control. Slow blockers such as peptides used to be an example of the competition model. They clearly share the same sites with the NH_2 terminus and typically induce a bi-exponential inactivation due to their low blocking rates.

It is interesting to know why the mutated construct FWI gives different dynamics in the period recovering from inactivation compared with the wild-type hβ2 (FIW). For FIW, the residue Trp-4, as the last residue involved in the inter-molecular interaction, is the most hindered component of the hydrophobic core maybe due to its large volume. It has less contact with the mouth of the channel (only one Ile-323) and is exposed to solvent. For construct FWI, the residue Trp-3 before Ile-4 as the second residue is also the most hindered component of the hydrophobic core. In comparison with FIW, the residue Trp-3 in FWI makes more contacts with the channels (interacting with two Ile-323 residues), is buried deeply and is less exposed to solvent. This kind of arrangement of the hydrophobic side chains in FWI might account for its distinct recovery behavior after inactivation. We expect that the last residue Ile-4 will firstly leave the pore at the beginning of the recovery, and then the buried residue Trp-3 will dissociate slowly with the Ile-323, which results in a slow recovery process. For construct FIW, the most hindered residue Trp-4 dissociates quickly due to the exposure to solvent and less interaction with the channel, and the residues Phe-2 and Ile-3 leave simultaneously to show monoexponential recovery process. This analysis may also explain why the complex *mSlo1*-FWQ shows identical recovery dynamics to that of the *mSlo1*-hβ2 complex. Because the glutamine (Gln) in the construct FWQ is a hydrophilic residue, the residue Trp-3 becomes solvent-exposed and so leads to a single exponential recovery. In complex I323A-FWI, the residue Ile-323 is replaced with a relatively weaker hydrophobic residue alanine, which leads to a reduced interaction between Trp-3 and Ile-323. Compared with the complex *mSlo1*-hβ2, the recovery of I323A-FWI shows a slight difference, which may be attributed to the shield effect of a following hydrophobic residue Ile-4.

It is interesting to consider why FWI shows a bi-exponential recovery with a 50:50 ratio. This feature may implicate that FWI has two interacting styles in the pore. At the recovery voltage of −140 mV with 10 μM Ca^{2+}, the ~50% of FWI may be trapped in a fast dissociating sub-state, which was not indicated in the present simulations of interaction between *mSlo* α and hβ2 subunits (Fig. 9), and the remaining half in a slow dissociating sub-state to lead to a bi-exponential recovery with a ratio of about 50:50. However, FIW has only one stable interaction style. The reason for that is probably that the rhombus-like FWI acts in an "unstable" style with two sub-states, but the cone-like FIW acts in a "stable" style with one state. Actually, the wide-type rβ2 (FIW) in rat chromaffin cells showed a much weaker bi-exponential recovery with a ratio of, on average, 25 (fast):75 (slow) at voltages more positive than −100 mV,[6] although the bi-exponential recovery of hβ2 (FIW) is extraordinarily rare. Obviously, more experiments are needed to verify whether the bi-exponential phenomena are ubiquitous in inactivating BK channels.

Acknowledgments—We thank Drs. C. J. Lingle and A. Wei for valuable comments on the manuscript and Drs. F. Qin and W. J. Cram for helpful discussions.

REFERENCES

1. Atkinson, N. S., Robertson, G. A., and Ganetzky, B. (1991) *Science* **253,** 551–555
2. Butler, A., Tsunoda, S., McCobb, D. P., Wei, A., and Salkoff, L. (1993) *Science* **261,** 221–224
3. Xia, X. M., Ding, J. P., and Lingle, C. J. (1999) *J. Neurosci.* **19,** 5255–5264
4. Wallner, M., Meera, P., and Toro, L. (1999) *Proc. Natl. Acad. Sci. U. S. A.* **96,** 4137–4142
5. Xia, X. M., Ding, J. P., Zeng, X. H., Duan, K. L., and Lingle, C. J. (2000) *J. Neurosci.* **20,** 4890–4903
6. Uebele, V. N., Lagrutta, A., Wade, T., Figueroa, D. J., Liu, Y., McKenna, E., Austin, C. P., Bennett, P. B., and Swanson, R. (2000) *J. Biol. Chem.* **275,** 23211–23218
7. Hoshi, T., Zagotta, W. N., and Aldrich, R. W. (1990) *Science* **250,** 533–538
8. Ruppersberg, J. P., Frank, R., Pongs, O., and Stocker, M. (1991) *Nature* **353,** 657–660
9. Rettig, J., Heinemann, S. H., Wunder, F., Lorra, C., Parcej, D. N., Dolly, J. O., and Pongs, O. (1994) *Nature* **369,** 289–294
10. Murrell-Lagnado, R. D., and Aldrich, R. W. (1993) *J. Gen. Physiol.* **102,** 949–975
11. Murrell-Lagnado, R. D., and Aldrich, R. W. (1993) *J. Gen. Physiol.* **102,** 977–1003
12. Xia, X. M., Ding, J. P., and Lingle, C. J. (2003) *J. Gen. Physiol.* **121,** 125–148

[6] J. Ding, unpublished data.

13. Demo, S. D., and Yellen, G. (1991) *Neuron* **7,** 743–753
14. Choi, K. L., Aldrich, R. W., and Yellen, G. (1991) *Proc. Natl. Acad. Sci. U. S. A.* **88,** 5092–5095
15. Zhou, M., Morais-Cabral, J. H., Mann, S., and MacKinnon, R. (2001) *Nature* **411,** 657–661
16. Lingle, C. J., Solaro, C. R., Prakriya, M., and Ding, J. P. (1996) *Ion Channels* **4,** 261–301
17. Solaro, C. R., Ding, J. P., Li, Z. W., and Lingle, C. J. (1997) *Biophys. J.* **73,** 819–830
18. Doyle, D. A., Morais Cabral, J., Pfuetzner, R. A., Kuo, A., Gulbis, J. M., Cohen, S. L., Chait, B. T., and Mackinnon, R. (1998) *Science* **280,** 67–99
19. Jiang, Y., Lee, A., Chen, J., Cadene, M., Chait, B. T., and MacKinnon, R. (2002) *Nature* **417,** 515–522
20. Long, S. B., Campbell, E. B., and MacKinnon, R. (2005) *Science* **309,** 897–903
21. Lippiat, J. D., Standen, N. B., and Davies, N. W. (2000) *J. Physiol.* **529,** 131–138
22. Bentrop, D., Beyermann, M., Wissmann, R., and Fakler, B. (2001) *J. Biol. Chem.* **276,** 42116–42121
23. Sakmann, B., and Neher, E. (1995) *Single-Channel Recording*, 2rd Ed., pp. 408–409, Plenum Press, New York
24. Li, W. Y., and Aldrich, R. W. (2004) *J. Gen. Physiol.* **124,** 43–57
25. Lingle, C. J., Zeng, X. H., Ding, J. P., and Xia, X. M. (2001) *J. Gen. Physiol.* **117,** 583–606
26. Zeng, X. H., Xia, X. M., and Lingle, C. J. (2003) *Nat. Struct. Biol.* **10,** 448–454
27. Lagrutta, A., Shen, K. Z., North, R. A., and Adelman, J. P. (1994) *J. Biol. Chem.* **269,** 20347–20351
28. Wei, A., Solaro, C., Lingle, C., and Salkoff, L. (1994) *Neuron* **13,** 671–681
29. Adelman, J. P., Shen, K. Z., Kavanaugh, M. P., Warren, R. A., Wu, Y. N., Lagrutta, A., Bond, C. T., and North, R. A. (1992) *Neuron* **9,** 209–216
30. Gao, Y. D., and Garcia, M. L. (2003) *Proteins* **52,** 146–154
31. McDonald, I. K., and Thornton, J. M. (1994) *J. Mol. Biol.* **238,** 777–793
32. Wallace, A. C., Laskowski, R. A., and Thornton, J. M. (1995) *Protein Eng.* **8,** 127–134
33. Gulbis, J. M., Zhou, M., Mann, S., and MacKinnon, R. (2000) *Science* **289,** 123–127
34. Benzinger, G. R., Xia, X. M., and Lingle, C. J. (2006) *J. Gen. Physiol.* **127,** 119–131